Molecular Mechanism of the *Z*/*E*-Photoisomerization of Hemithioindigo Hemistilbene†

J. Plötner and A. Dreuw*

Institut für Physikalische und Theoretische Chemie, Johann Wolfgang Goethe-Universität, Max von Laue-Str. 7, 60438 Frankfurt am Main, Germany

Received: April 6, 2009; Revised Manuscript Received: September 4, 2009

Hemithioindigo hemistilbene (HTI) can be selectively photoisomerized from the *Z*-isomer into the *E*-isomer and vice versa. Using quantum chemical calculations, we have investigated the mechanism of the photoisomerization in detail. Our calculations demonstrate that two *Z*- and *E*-isomers exist in the electronic ground state as well as on the S_1 surface. The S_1 isomers are separated by small energy barriers along the dihedral twisting coordinate, but also a conical intersection with the electronic ground state is present at about 90° twisting angle. Comparison with previously published experimental data reveals that most excited molecules, however, do not isomerize but instead relax to the equilibrium structure of the *Z*-isomer on the S_1 surface and return back to the ground state via regular fluorescence. Only a small fraction of the excited state population decays via the identified conical intersection and forms ground state *E*-isomers. This explains the comparably long lifetime of 38 ps of the excited HTI molecules and the observed low quantum yield of photoswitching.

I. Introduction

Photoswitches are molecules that exist in two distinct states with different physical properties and that can be reversibly switched from one state into the other by photoexcitation. One of the most prominent examples is azobenzene, which is well-known to undergo ultrafast cis−trans photoisomerization within a few hundred femtoseconds.[1−5] It isomerizes from the thermodynamically most stable trans-conformation to the cis-form upon excitation with light of 360 nm, and backward when the cis-isomer is excited with 430 nm; i.e., azobenzene can even be isomer-selectively switched.[1] The large difference of the spatial extension of trans- and cis-azobenzene is successfully employed in several applications to phototrigger the folding and unfolding of proteins with embedded azobenzene-based photoswitches.[6,7] In general, the possibility to phototrigger selectively a drastic change of physical properties of molecules, as for example, refractive index, spatial extension, dipole moment, etc. allows for plenty technical applications. Azobenzenes, for instance, are considered as potential materials for optical data storage devices.[8−10]

In nature, photoswitches are usually employed for sensing light. Human vision relies on the photoisomerization of retinal, the chromophore of rhodopsin. It undergoes ultrafast photoisomerization from the 11-cis to the all-trans-form,[11] introducing a perturbation that eventually leads to protein rearrangement and signal transduction. The same is true for the photoactive yellow protein of purple bacteria, which is responsible for negative phototaxis.[12] Here, *p*-coumaric acid acts as photoswitch, which is photoisomerized from the trans- to the cis-isomer finally triggering a protein response producing a signal that makes the bacteria avoid UV light.[13] In these biological cases, however, the back-isomerization is not triggered by a photon but takes place thermally in the electronic ground state.

Recently, large experimental and theoretical efforts have been made to discover new molecular photoswitches, among those are hemithioindigo hemistilbene (HTI) (Figure 1) and substituted derivatives thereof,[14−17] which are structurally closely related to stilbene.[14] It has been observed that HTI can be switched from the thermodynamically most stable *Z*-isomer to the *E*-isomer upon excitation into the S_1 state and that a photostationary equilibrium can be reached where as much as 95% of all molecules are in the *E*-form. It is well established that the *Z*- and *E*-isomers have absorption maxima at λ_{max} of 430 nm and 460 nm, respectively.[17]

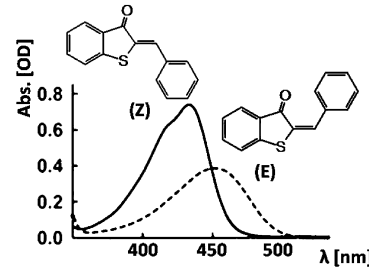

Figure 1. Molecular structure of the *Z*- and *E*-isomers of hemithioindigo (HTI) and their corresponding experimental absorption spectra.[17]

A detailed investigation of the HTI photoisomerization employing ultrafast time-resolved transient absorption spectroscopy revealed the kinetics of that process.[17] For a proper description of the observed kinetics three monoexponential functions are required exhibiting time constants of 300 fs, 2.3 ps, and 38 ps, respectively. On the basis of the experimental findings and motivated by the structural relation of HTI to stilbene, a model for the decay mechanism was proposed. It is assumed that the fastest decay process represents the relaxation of the initially created excited state population out of the Franck−Condon region into the equilibrium structure of the *Z*-isomer on the S_1 potential energy surface. The second decay component is proposed to correspond to further decay of the *Z*-isomer into a twisted structure still on the S_1 surface with substantial charge-transfer (CT) character. The slowest decay component finally describes the decay of the latter CT state into both *Z*- and *E*-isomers now back in the electronic ground state.

† Part of the "Walter Thiel Festschrift".

* Corresponding author. URL: http://http://www.theochem.uni-frankfurt.de/quantchem. Electronic address: andreas.dreuw@theochem.uni-frankfurt.de.

10.1021/jp903156j CCC: $40.75
Published on Web 09/28/2009

TABLE 1: Comparison of the Excitation Wavelengths of the Four Lowest Excited States of the *Z*-Isomer of HTI at BLYP, B3LYP, BHLYP, CIS, and ADC(2) Levels of Theory[a]

	BLYP		B3LYP		BHLYP		CIS		ADC(2)		
state	ω_{ex}	osc	ω_{ex}	osc	ω_{ex}	osc	ω_{ex}	osc	ω_{ex}	osc	character
S1	490	0.15	415	0.22	341	0.34	265	0.30	369	0.39	$\pi\pi^*$
S2	449	0.00	375	0.00	313	0.00	250	0.00	355	0.00	$n\pi^*$
S3	373	0.15	315	0.28	267	0.43	227	0.15	263	0.72	$\pi\pi^*$
S4	357	0.00	297	0.00	248	0.02	212	0.00	257	0.01	$\pi\pi^*$(CT)

[a] The excitation wavelengths (ω_{ex}) are given in nm. The character of the states is the same at all levels of theory.

In this work, we perform high-level quantum chemical calculations to investigate the molecular mechanism of the *Z*/*E*-photoisomerization pathway of unsubstituted HTI. Our calculations reveal that nonplanar *Z*- and *E*-isomers are both present already on the S_1 surface. However, most of the excited state population does not isomerize but decays via regular fluorescence out of the relaxed *Z*-isomer back to the electronic ground state. Only a small fraction of the excited HTI molecules reaches a conical intersection with the electronic ground state efficiently and forms ground state *E*-isomers. This explains the comparably long lifetime of most of the excited HTI molecules of 38 ps compared to the very short one of only about 200 fs of excited azobenzene molecules.

II. Computational Details

The investigation of the *Z*/*E*-photoisomerization comprises the optimization of the structure of the *Z*- and *E*-isomers in the electronic ground and first excited states as well as the calculation of the vertical excitation spectra at these stationary points. For all computations the Q-Chem 3.2[18] and Turbomole 5.10 program packages[19] have been employed.

For the calculation of the vertical excited states of HTI, time-dependent density functional theory (TDDFT)[20,21] and the algebraic diagrammatic construction scheme of second order (ADC(2))[22−24] has been used. Unfortunately, HTI is already quite large, allowing us to use ADC(2) only for benchmarking TDDFT results, and not for optimization of the excited state structures and relaxed scans of the potential energy surfaces. Thus one has to resort to the computationally cheaper TDDFT.

TDDFT generally exhibits problems with charge-transfer (CT) exited states;[25−27] however, the correct description of which is important for the investigation of the HTI photoisomerization. As a first step, we thus performed a thorough study of the dependence of the TDDFT excited state calculations on basis set size and exchange−correlation (xc)-functional. It was found that the excitation energies of the relevant four lowest excited state are practically independent of the basis set size. Hence we decided to use Dunning's double- ζ basis set plus polarization functions (DZP) as implemented in Turbomole[19] as the standard in our TDDFT calculations. All tested xc-functionals (BLYP,[28,29] B3LYP,[30,29] BHLYP[31]) yielded the same state ordering at the planar ground state equilibrium structures of the *Z*- and *E*-isomers of HTI (Table 1). Since no spurious intruder CT states have been identified using the BLYP xc-functional, problems arising from the CT failure of TDDFT can be excluded for the calculation of the vertical excited states in the case of HTI. The excitation energies, however, show the expected shift to higher values with increasing amounts of nonlocal Hartree−Fock exchange (Table 1). In an earlier study, we have observed that xc-functionals with no or only a low fraction of HF exchange can result in spurious minima on the potential energy surface of excited states, even when the vertical excitation energies are well described.[27] Typically, these artificial minima correspond to twisted structures with high charge-transfer character as revealed by an unnaturally high excited state static dipole moment.[27] To obtain reliable excited state geometries for HTI, we thus decided to use the BHLYP functional for the excited state geometry optimizations and the calculation of a relaxed scan along the *Z*/*E*-isomerization pathway on the S_1 surface. For consistency, we then also optimized the ground state structures with DFT using also the BHLYP functional. All identified stationary points on the ground and excited state surfaces have been checked by frequency analyses revealing no imaginary frequencies.

The influence of the solvent on the vertical excited states of HTI has been checked by application of the COSMO model within the TDDFT/BHLYP calculations.[32,33] We have used a dielectric constant of $\varepsilon = 32.6$ to model methanol, the solvent employed in the corresponding experiment.[17] However, the influence of the solvent appears to be negligible. The vertical excitation energy of the ground state *Z*-isomer of HTI changes from 3.62 to 3.59 eV and that of the *E*-isomer from 3.43 to 3.41 eV when COSMO is used. The changes in the excitation energies of the other energetically low-lying excited states are similarly small. Thus, we do generally not include the COSMO model in our standard calculations.

III. Numerical Results

A. Ground State Properties and Static Absorption Spectra. Geometry optimizations on the electronic ground state surface of HTI confirmed the existence of one stable *Z*- and one stable *E*-isomer, which are depicted in Figure 1 and whose relevant geometrical parameters are given in Table 2. Both ground state isomers are planar, exhibiting S−C═C−C dihedral angles at the central isomerizing double bond of 0.18° (*Z*) and 179.9° (*E*), respectively. Due to steric repulsion, the C═C−C bond angle between this central double bond and the carbon of the phenyl ring deviates slightly from the expected 120° value for sp2-hybridized carbon atoms and is enlarged to around 135° in both isomers. The static dipole moment of both isomers is moderate with values of 2.33 and 1.35 Debeye for the *Z*- and *E*-isomers (Table 2). In the electronic ground state, the *Z*-isomer is found to be lower in energy than the *E*-isomer at all employed levels of theories. At the MP2/6-31G* and DFT/BHLYP/DZP level, the energy difference between *Z* and *E* is practically identical with a value of 17.6 kJ mol^{-1}; i.e., in thermal equilibrium 99.9% of the HTI molecules are *Z*-isomers according to a Boltzmann distribution. At ambient conditions no evidence for the presence of *E*-isomers in thermal equilibrium has been found in spectroscopic investigations.[17]

Turning to the calculation of the vertical excited states of the *Z*- and *E*-isomers, the computed excitation energies, their oscillator strengths and character is compiled in Table 1. The lowest excited S_1 state is an optically allowed $\pi\pi^*$ state with an oscillator strength of 0.34 at the level of TDDFT/BHLYP, which is represented by a transition from the highest occupied

TABLE 2: Significant Geometrical Parameters, Relative Energies of the Ground State and Excited State (rel $E(S_0)$ and rel $E(S_1)$), Vertical Excitation Energies and Excitation Wavelengths (ω) of the *Z*- and *E*-Isomers of HTI Optimized in the Electronic Ground ($Z(S_0)$ and $E(S_0)$) and Optimized in the First Excited Electronic State ($Z(S1)$ and $E(S1)$)[a]

	$Z(S_0)$	$Z(S_1)$	$E(S_0)$	$E(S_1)$
S−C═C−C dihedral angle (deg)	0.0	20.0	180.0	157.3
C═C−C angle (deg)	132.2	130.6	135.7	125.8
C═C bond length (Å)	1.33	1.39	1.35	1.39
rel $E(S_0)$ (eV)	0.00	+0.30	+0.18	+0.72
rel $E(S_1)$ (eV)	+0.25	+0.05	+0.24	0.00
ω_{theo} (S_1) (eV)	3.62	3.13	3.43	2.65
ω_{theo} (S_1) (nm)	341	396	361	467
ω_{expt} (S_1) (eV)	2.88	2.53	2.75	
ω_{expt} (S_1) (nm)	430	490	450	
ω_{shift} (S_1) (eV)	2.88	2.39	2.69	1.91
ω_{shift} (S_1) (nm)	430	518	460	649

[a] For the excitation energies and wavelengths, values at the TDDFT/BHLYP level of theory (ω_{theo}) and experimentally determined values (ω_{expt}) are given; 0.74 eV red-shifted theoretical values (ω_{shift}) are also given (see text).

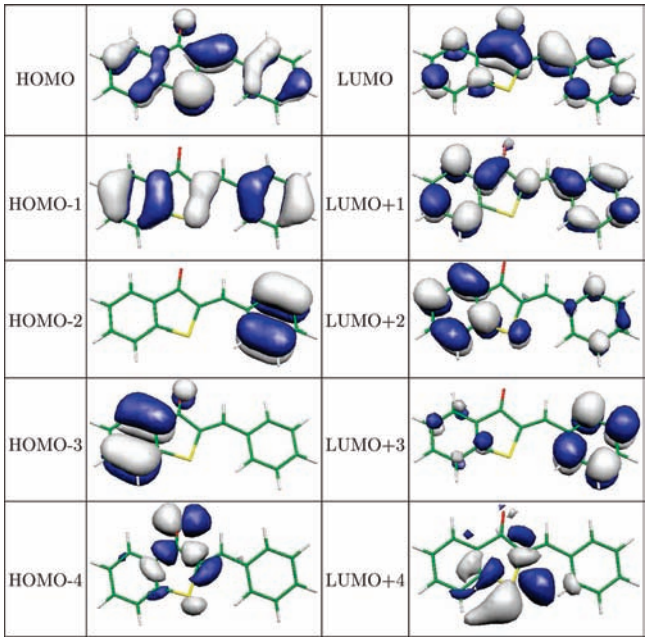

Figure 2. Molecular valence orbitals of HTI computed at the TDDFT/BHLYP/DZP level of theory.

molecular orbital (HOMO) to the lowest unoccupied molecular orbital (LUMO). The relevant valence orbitals of HTI as obtained by DFT/BHLYP/DZP are displayed in Figure 2. The second lowest excited S_2 state of HTI corresponds to an $n\pi^*$ transition, where the n-orbital is a lone pair of the carbonyl oxygen of HTI. This state is best described as excitation of an electron from the HOMO−4 into the LUMO (Figure 2). The S_3 state is again a $\pi\pi^*$ transition best represented as a one-electron transition from the HOMO−1 into the LUMO. The S_4 state is also essentially of $\pi\pi^*$ nature; however, it exhibits some charge-transfer character, in which electron density is transferred from the phenyl ring to the central five-membered ring. This can be easily seen when the involved orbitals are inspected, since the S_4 state is well described as excitation of an electron from the HOMO−2 into the LUMO (see Figure 2). It is important to note that this CT state is not an artifact of the TDDFT method, since it is also present at the level of configuration interaction singles (CIS) and ADC(2), which both describe CT states physically correct.

The calculated excitation energies exhibit the typical errors of the applied methods. The excitation energy of the lowest S_1 $\pi\pi^*$ state of the *Z*-isomer of HTI is 0.74 eV overestimated at the level of TDDFT/BHLYP, 0.12 eV overestimated at the level of TDDFT/B3LYP, and 0.3 eV underestimated at the level of TDDFT/BLYP. Although the computed excitation energy is in much better agreement with the experimental value when the B3LYP xc-functional is employed in the TDDFT calculation than with the BHLYP xc-functional, we will use the BHLYP xc-functional for the excited state geometry optimization to avoid the occurrence of artificial minima on the potential energy surface as observed previously.[27]

B. Excited State Properties and Fluorescence Spectra. For the calculation of the excited state properties and the fluorescence spectra, the structures of the *Z*- and *E*-isomers have been optimized in the S_1 excited state using TDDFT with the BHLYP xc-functional and DZP basis set. Indeed, two local minima exist also on the S_1 potential energy surface corresponding to slightly twisted *Z*- and *E*-isomers. No other stable equilibrium structures of HTI have been found on the S_1 surface. In detail, the S−C═C−C dihedral angle at the central double bond of HTI exhibits values of 20° and 157° in the *Z*- and *E*-isomers (Table 2). The slight twisting of the central dihedral angle removes some of the steric hindrance such that the corresponding C═C−C angle becomes slightly smaller in the S_1 equilibrium structures. On the other hand, the central double bond is elongated by 0.05 Å in the excited state structures compared to the ones in the electronic ground state. This can be explained by an additional node of the LUMO at that double bond (Figure 2), since an electron is excited in S_1 from the HOMO to the LUMO, resulting in a decrease of bond order. This clearly facilitates also the isomerization from *Z* to *E* on the excited S_1 state surface.

In contrast to the ground state, the *E*-isomer is slightly more stable than the *Z*-isomer on the S_1 surface. The energy difference is very small with a value of only 4.9 kJ mol^{-1} at the theoretical level of TDDFT/BHLYP/DZP. The static dipole moments of both isomers are also practically identical with the *Z*- and *E*-isomers exhibiting values of 4.56 and 4.67 Debeye. Assuming Kasha's rule that fluorescence occurs out of the relaxed excited state structures, the fluorescence wavelengths of the *Z*- and *E*-isomers can be calculated as the vertical excitation energies at the optimized S_1 geometries. At the level of TDDFT/BHLYP/DZP, these amount to 3.13 and 2.65 eV resulting in fluorescence wavelengths of 396 and 467 nm for the *Z*- and *E*-isomer of HTI. The corresponding oscillator strengths of the S_1 state at the geometry of the *Z*- and *E*-isomers are 0.35 and 0.18, respectively. The experimentally determined fluorescence wavelength for the *Z*-isomer is 490 nm, corresponding to an excitation energy of 2.53 eV. It is worthwhile to note that the error of 0.6 eV compared to the experimental value is about the same as the one of the computed absorption wavelength. It seems that the deviations between the calculated vertical excitation energies and their corresponding experimental values are very similar for each identified equilibrium structure. Thus, we have shifted all computed TDDFT/BHLYP excitation energies by 0.74 eV to lower energies, which is the deviation between the measured and calculated vertical excitation energy of the ground state *Z*-isomer. In other words, the calculated values are normalized with respect to the measured vertical excitation energy of the ground state *Z*-isomer. This procedure yields shifted, semitheoretical values of 2.39, 2.69, and 1.91 eV for the excitation

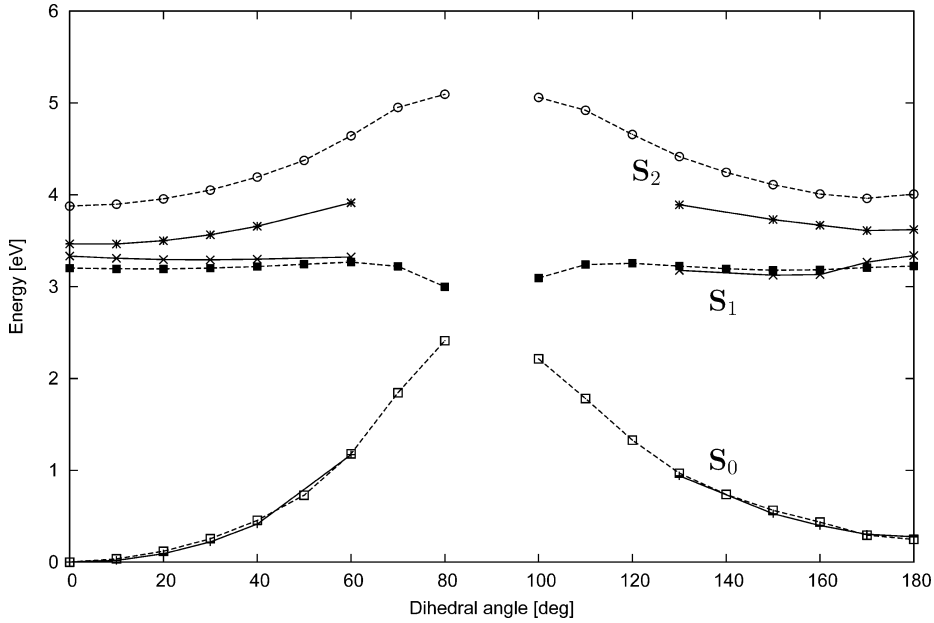

Figure 3. Relaxed scan of the S_1 potential energy surface for the *Z*/*E*-photoisomerization of HTI. The central S−C═C−C dihedral angle was fixed while all other parameters were reoptimized on the S_1 surface employing TDDFT/BHLYP/DZP. The TDDFT curves are given as dashed lines, while ADC(2) curves calculated as single points along the path are given as solid lines.

energies of the *Z*-isomer on the S_1 surface and the *E*-isomers on the ground state and excited S_1 state surface, respectively. Compared to the known experimental values, the errors are very small: 0.14 eV for the excited S_1 state *Z*-isomer and only 0.06 eV for the ground state *E*-isomer of HTI.

IV. Mechanism of the *Z*/*E*-Photoisomerization of HTI

To understand the photoinitiated *Z*/*E*-isomerization of HTI upon excitation into the S_1 state, the potential energy surfaces of the ground and excited S_1 state have been computed along the S−C═C−C dihedral angle, which corresponds to the traditional one-bond-flip mechanism. We have initially also tested the Hula-twist mechanism by calculation of first steps of a relaxed scan; however, the energy increases quite steeply along this path, indicating that it is not relevant for the isomerization mechanism and for the explanation of the experimental observations. Therefore, we have restricted ourselves to the investigation of the classical one-bond-flip mechanism. For this objective, two conceptually different reaction pathways were chosen. First, the potential energy surfaces have been calculated along the dihedral twisting coordinate starting at the optimized ground state structure of the *Z*-isomer without reoptimization of the geometry along the path. The resulting pathway can be understood as an infinitely fast photoreaction, during which all other geometrical parameters have no time to adjust. This pathway will be referred to as the instantaneous pathway. Second, the relaxed scan for the photoisomerization along the S−C═C−C dihedral angle twisting coordinate has been computed, allowing all other geometrical parameters to freely relax along the path on the S_1 surface. This reaction path would then correspond to an infinitely slow reaction, since all geometrical parameters have infinite time to adopt their equilibrium values during the reaction. Both chosen pathways represent two extreme cases, and by studying both, one gains insight into the importance of relaxation effects. In the case of HTI, the potential energy curves of both pathways look practically identical, and only the relaxed scan is depicted in Figure 3.

Besides the two minima on the S_1 surface, the presence of a conical intersection could be identified at a dihedral angle of around 90°. In the vicinity of the conical intersection the ground state DFT calculation cannot converge onto a stable solution explaining the gap in Figure 3 around 90°. However, also a barrier is present along the relaxed scan with a value of 0.07 eV, which excited *Z*-isomers must surpass to reach the conical intersection. Along the instantaneous isomerization path, the barrier is naturally higher and has a value of 0.21 eV. Detailed analysis of changes of other geometrical parameters reveals that the carbon atom of the central double bond bound to the phenyl ring pyramidalizes along the relaxed scan, which leads to the decrease of the barrier from 0.21 to 0.07 eV upon geometry reoptimization. The transition state between the *Z*-isomer and the conical interection occurs at an S−C═C−C dihedral angle of 60° and possesses a C═C−C angle of 125° and a C═C bond length of 1.41 Å. The transition state connecting the *E*-isomer and the conical intersection is characterized by a dihedral angle of 120.1°, an angle of 124.7°, and a C═C bond length of also 1.41 Å. All other geometrical parameters are practically identical to the ones of the optimized equilibrium structures of the *Z*- and *E*-isomers. To confirm the DFT and TDDFT results, single-point ADC(2)-s calculations have been performed. As can be seen in Figure 3, the ADC(2)-s curves exhibit the same shape and practically identical energetics of the S_0 and S_1 state as the ones computed with TDDFT/BHLYP.

In view of our findings, recent results of time-resolved transient absorption spectroscopy[17] and hence the mechanism of the *Z*/*E*-isomerization of HTI can be understood as follows. Upon photoexcitation, the excited state population moves out of the Franck−Condon region. This process is experimentally identified to occur via 300 fs. As already mentioned in the Introduction, two further monoexponential functions with time constants of 2.3 and 38 ps are required to describe the excited state dynamics.[17] Taking our theoretical findings into account, the experimentally determined main component with a lifetime of 38 ps is now straightforwardly to identify as *Z*-isomer on the S_1 surface, which repopulates the ground state *Z*-isomer via fluorescence. The corresponding decay associated spectrum of that kinetic component (see Figure 3 of ref 17) exhibits the expected ground state recovery signal at about 430 nm and the

fluorescence signature around 490 nm. This kinetic component cannot correspond to the *E*-isomer on the S_1 surface, since its fluorescence should occur around 650 nm according to our calculations.

Most problematic is the interpretation of the kinetic component with a lifetime of 2.3 ps. In its decay associated spectrum (see Figure 3 in ref 17), two negative contributions are apparent at around 450 and 500 nm, and no ground state recovery signal of the *Z*-isomer at 430 nm can be seen. Since our calculation revealed only the two *Z*- and *E*-isomers on the S_1 surface, this kinetic component can only correspond to one of them. The negative contribution at 450 nm can be explained with the population of the ground state *E*-isomer, which absorbs at this wavelength. The negative contribution at 500 nm representing increasing absorption occurs exactly where the excited *Z*-isomer (the 38 ps component) has the maximum of its excited state absorption. Thus, some population of the 2.3 ps kinetic component decays also into the population corresponding to the kinetic component with 38 ps lifetime.

These spectral features and kinetic behavior can be explained to stem from vibrationally excited (hot) HTI *Z*-isomers. Some part of that population reaches the conical intersection and generates ground state *E*-isomers, and some part cools further down, i.e., relaxes into the equilibrium structure of the *Z*-isomer on the S_1 surface and decays eventually via fluorescence within 38 ps. This would explain both negative contributions at 450 nm and around 500 nm, and the slightly red-shifted excited state absorption of that population as compared to the one of the 38 ps component.

It is unlikely that this 2.3 ps component corresponds to a population of the *E*-isomer on the S_1 surface that may return to the ground state via fluorescence and which would also have to repopulate the *Z*-isomer equilibrium to explain both negative contributions in its decay associated spectrum. Although the fluorescence would most likely not have been detected in the experiment due to its large red-shift, one may wonder how the excited *Z*-molecules isomerize on the S_1 surface into *E*-isomers without going through the conical intersection to efficiently populate the ground state. And even if they could do so, why should excited *E*-isomers return back to the *Z*-configuration, for the former is slightly lower in energy than the latter on the S_1 surface.

Summarizing the mechanism of the HTI photoisomerization, upon excitation the created S_1 *Z*-population moves out of the Franck−Condon region within about 300 fs. Only the *Z*-isomer is populated on the S_1 surface; however, it decays via two processes. A vibrationally excited part of the population goes through the identified conical intersection and forms ground state *E*-isomers within 2.3 ps, while the largest part of the whole excited state population obeys Kasha's rule and fluoresces out of the equilibrium structure of the *Z*-isomer with a lifetime of 38 ps.

Apparently, the excited state dynamics of HTI are dominated by two competing processes: regular fluorescence and *E*/*Z*-photoisomerization. The efficiency of photoisomerization is regulated on one hand by the height of the energy barrier that separates the equilibrium structure of the *Z*-isomer on the S_1 surface from the conical intersection leading to the ground state *E*-isomer. On the other hand, it is decisive how efficient kinetic energy is funnelled into the reaction coordinate, i.e., dihedral twisting, upon photoexcitation. In the case of HTI, the Franck−Condon point lies above the barrier and the initial energy is in principle sufficient to overcome it. However, the observed time scales and the assignment of the intermediates suggests that only a small fraction of the excited population has initially enough energy in the reaction coordinate to pass the barrier quickly. For the most part of the population, the energy in the reaction coordinate is obviously initially not sufficient and internal energy redistribution (IVR) into the reaction coordinate seems too slow for photoisomerization to efficiently compete with fluorescence. To clarify these subtleties of the photoisomerization mechanism of HTI, elaborate quantum dynamical calculations would be necessary. These are currently, however, out of reach for contemporary theoretical chemistry due to the size of the HTI molecule and the high dimensionality of the dynamics. Further experiments like excitation energy dependent measurements of the photoisomerization efficiency would also help to clarify this issue. Since an energy barrier is involved in the photoisomerization of HTI, one may expect the efficiency to increase with increasing excitation energy.

V. Brief Summary and Conclusions

Recent experiments employing time-resolved femto-second spectroscopy have shown that hemithioindigo (HTI) can be selectively photoisomerized from the stable *Z*-isomer to the *E*-form.[17] Here, we have employed high-level quantum chemical methods to thoroughly study the mechanism of the *Z*/*E*-photoisomerization of HTI. Our calculations demonstrate that both *Z*- and *E*-configurations correspond to stable isomers in the electronic ground state, but also in the first excited state. No other equilibrium structures could be identified on the S_1 surface, in particular, none with substantial charge-transfer character. While the *Z*-form is clearly more stable than the *E*-isomer in the electronic ground state, they are practically degenerate in the S_1 state with the *E*-isomer being slightly more stable. The calculated absorption and fluorescence wavelengths agree very favorably with the experimentally known values.

Investigation of the potential energy surfaces of the electronic ground and excited S_1 state along the twisting coordinate of the central S−C═C−C dihedral angle, the most probable isomerization coordinate, demonstrates that it is dominated by the two *Z*- and *E*-isomers and a conical intersection at about 90° twisting angle. Between the minimum of the *Z*-isomer and the conical intersection a small energy barrier of 0.075 eV has been identified along the relaxed scan.

In view of these findings and taking recent experiments into account, the mechanism of photoisomerization of HTI can be understood as follows. Upon photoexcitation the excited state population relaxes rapidly out of the Franck−Condon region toward the equilibrium structure of the *Z*-isomer on the S_1 surface. While a small fraction has enough energy to quickly reach the conical intersection and thus to isomerize into the ground state *E*-form, most of the excited state population gets trapped in the minimum of the *Z*-isomer and decays back to the ground state via regular fluorescence obeying Kasha's rule.

In our quantum chemical investigation, we focused on the unsubstituted HTI chromophore; however, also substituted HTI derivatives have been investigated experimentally.[14−17] It has been shown that substitution does have an influence on the isomerization time scale and the yield of *E*-isomers. However, preliminary calculations of the relative energies of the *Z*- and *E*-isomers of substituted derivatives in the S_1 excited state, reveals that para-substitution with bromine, chlorine, cyano, or methoxy groups has a negligible influence and that the *E*-isomer remains about 0.05−0.06 eV more stable than the *Z*-isomer. But also for these molecules, no other stable isomer could be identified on the S_1 surface. For a detailed understanding of the observed differences, the heights of the involved barriers and

the role of the conical intersection need to be determined for each of the substituted derivatives. A throrough study addressing these subtle differences between the substituted derivatives of HTI is currently under way; however, to obtain the required accuracy, other theoretical methods like CASSCF need additionally to be taken into account that allow for a precise location of the conical intersection.

Acknowledgment. We thank Prof. Wolfgang Zinth for pointing us to the interesting photochemistry of HTI. A.D. acknowledges financial support as Heisenberg-Professor of the Deutsche Forschungsgemeinschaft.

References and Notes

(1) Nägele, T.; Hoche, R.; Zinth, W.; Wachtveitl, J. *Chem. Phys. Lett.* **1997**, *272*, 489–495.
(2) Bredenbeck, J.; Helbig, J.; Sieg, A.; Schrader, T.; Zinth, W.; Renner, C.; Behrendt, R.; Moroder, L.; Hamm, P. *Proc. Natl. Acad. Sci. U.S.A.* **2003**, *100*, 6452–6457.
(3) Schultz, T.; Quenneville, J.; Levinne, B.; Toniolo, A.; Martinez, T. J.; Lochbrunner, S.; Schmitt, M.; Schaffer, J. P.; Zgierski, M. Z.; Stolow, A. *J. Am. Chem. Soc.* **2003**, *125*, 8098–8099.
(4) Cembran, A.; Bernardi, F.; Garavelli, M.; Gagliardi, L.; Orlandi, G. *J. Am. Chem. Soc.* **2004**, *126*, 3234–3243.
(5) Henzl, J.; Mehlhorn, M.; Gawronski, H.; Riedler, K. H.; Morgenstern, K. *Angew. Chem., Int. Ed.* **2006**, *45*, 603.
(6) Spörlein, S.; Carstens, H.; Renner, C.; Behrendt, R.; Moroder, L.; Tavan, P.; Zinth, W.; Wachtveitl, J. *Proc. Natl. Acad. Sci.* **2002**, *99*, 7998.
(7) Wachtveitl, J.; Spörlein, S.; Satzger, H.; Fonrobert, B.; Renner, C.; Behrendt, R.; Oesterhelt, D.; Moroder, L.; Zinth, W. *Biophys. J.* **2004**, *86*, 2350.
(8) Ikeda, T.; Ichimura, K. *Nature* **1993**, *361*, 428.
(9) Cheben, P.; del Monte, F.; Worsfold, D. J.; Carlsson, D. J.; Grover, C. P.; Mackenzie, J. D. *Nature* **2000**, *408*, 64.
(10) Åstrand, P. O.; Ramanujam, P. S.; Hvilsted, S.; Bak, K. L.; Sauer, S. P. A. *J. Am. Chem. Soc.* **2000**, *122*, 3482.
(11) Nakamichi, H.; Okada, T. *Angew. Chem., Int. Ed. Engl.* **2006**, *45*, 4270.
(12) Kort, R.; Vonk, H.; Xu, X.; Hoff, W. D.; Crielaard, W.; Hellingwerf, K. J. *FEBS Lett.* **1996**, *382*, 73.
(13) Hoff, W. D.; van Stokkum, I. H. M.; van Ramesdonk, H. J.; van Brederode, M. E.; Brower, A. M.; Fitch, J. E.; Meyer, T. E.; van Grondelle, R.; Hellingwerf, K. J. *Biophys. J.* **1994**, *67*, 1691.
(14) Cordes, T.; Weinrich, D.; Kampa, S.; Riesselmann, K.; Herre, S.; Hoppmann, C.; Rück-Braun, K.; Zinth, W. *Chem. Phys. Lett.* **2006**, *428*, 5167.
(15) Cordes, T.; Heinz, B.; Regner, N.; Hoppmannn, C.; Schroeder, T. E.; Summer, W.; Rück-Braun, K.; Zinth, W. *Chem. Phys. Chem* **2007**, *8*, 1713–1721.
(16) Cordes, T.; Schadendorf, T.; Priewisch, B.; Rück-Braun, K.; Zinth, W. *J. Phys. Chem. A* **2008**, *112*, 581.
(17) Cordes, T.; Schadendorf, T.; Rück-Braun, K.; Zinth, W. *Chem. Phys. Lett.* **2008**, *455*, 197–201.
(18) Shao, Y.; Molnar, L. F.; Jung, Y.; Kussmann, J.; Ochsenfeld, C.; Brown, S. T.; DiStasio, R. A., Jr.; Gilbert, A. T. B.; Slipchenko, L. V.; Levchenko, S. V.; O'Neill, D. P.; Lochan, R. C.; Wang, T.; Beran, G. J. O.; Besley, N. A.; Herbert, J. M.; Lin, C. Y.; Voorhis, T. V.; Chien, S. H.; Sodt, A.; Steele, R. P.; Rassolov, V. A.; Maslen, P. E.; Korambath, P. P.; Adamson, R. D.; Austin, B.; Baker, J.; Byrd, E. F. C.; Dachsel, H.; Doerksen, R. J.; Dreuw, A.; Dunietz, B. D.; Dutoi, A. D.; Furlani, T. R.; Gwaltney, S. R.; Heyden, A.; Hirata, S.; Hsu, C.-P.; Kedziora, G.; Khalliulin, R. Z.; Klunzinger, P.; Lee, A. M.; Lee, M. S.; Liang, W.; Lotan, I.; Nair, N.; Peters, B.; Proynov, E. I.; Pieniazek, P. A.; Rhee, Y. M.; Ritchie, J.; Rosta, E.; Sherrill, C. D.; Simmonett, A. C.; Subotnik, J. E.; Woodcock, H. L., III; Zhang, W.; Bell, A. T.; Chakraborty, A. K. *Phys. Chem. Chem. Phys.* **2006**, *8*, 3172–3191.
(19) TURBOMOLE V6.0 2009, a Development of the University of Karlsruhe and the Forschungszentrum Karlsruhe GmbH, 1989−2007, TURBOMOLE GmbH, since 2007; available from http://www.turbomole.com.
(20) Casida, M. E. In *Recent Advances in Density Functional Methods*; Chong, D. P., Ed.; World Scientific: Singapore, 1995; Part I, pp 155−192.
(21) Dreuw, A.; Head-Gordon, M. *Chem. Rev.* **2005**, *105*, 4009.
(22) Trofimov, A. B.; Schirmer, J. *J. Phys. B* **1995**, *28*, 2299.
(23) Schirmer, J.; Trofimov, A. B. *J. Chem. Phys.* **2004**, *120*, 11449.
(24) Starcke, J. H.; Wormit, M.; Schirmer, J.; Dreuw, A. *Chem. Phys.* **2006**, *329*, 39.
(25) Dreuw, A.; Weisman, J. L.; Head-Gordon, M. *J. Chem. Phys.* **2003**, *119*, 2943–2946.
(26) Dreuw, A.; Head-Gordon, M. *J. Am. Chem. Soc.* **2004**, *126*, 4007–4016.
(27) Plötner, J.; Dreuw, A. *Chem. Phys.* **2008**, *347*, 427.
(28) Becke, A. D. *Phys. Rev. A* **1988**, *38*, 3098–3100.
(29) Lee, C.; Yang, W.; Parr, R. G. *Phys. Rev. B* **1988**, *37*, 785.
(30) Becke, A. D. *J. Chem. Phys.* **1993**, *98*, 5648.
(31) Becke, A. D. *J. Chem. Phys.* **1993**, *98*, 1372.
(32) Klamt, A.; Schüürmann, G. *J. Chem. Soc., Perkin Trans. 2* **1993**, 799.
(33) Klamt, A. *J. Phys. Chem.* **1996**, *100*, 3349.

JP903156J